HYBRID TESTING OF COMPOSITE STRUCTURES WITH SINGLE-AXIS CONTROL

J. Waldbjørn[1], J. Høgh[2]*, H. Stang[1], C. Berggreen[2], J. Wittrup-Schmidt[1],
K. Branner[3]

[1]Department of Civil Engineering, Technical University of Denmark, Kgs. Lyngby, Denmark
[2]Department of Mechanical Engineering, Technical University of Denmark, Kgs. Lyngby, Denmark
[3]Department of Wind Energy, Technical University of Denmark, Roskilde, Denmark
* Corresponding author jhho@dtu.dk

Keywords: *hybrid testing, hardware-in-the-loop, substructural testing, composites, three point bending, finite element modelling, high-precision control*

Abstract

Hybrid testing is a substructuring technique where a structure is emulated by modelling a part of it in a numerical model while testing the remainder experimentally. Previous research in hybrid testing has been performed on multi-component structures e.g. damping fixtures, however in this paper a hybrid testing platform is introduced for single-component hybrid testing. In this case, the boundary between the numerical model and experimental setup is defined by multiple Degrees-Of-Freedoms (DOFs) which highly complicate the transferring of response between the two substructures. Digital Image Correlation (DIC) is therefore implemented for displacement control of the experimental setup. The hybrid testing setup was verified on a multicomponent structure consisting of a beam loaded in three point bending and a numerical structure of a frame. Furthermore, the stability of the hybrid testing loop was investigated for different ratios of stiffness between the numerical model and test specimen. It was found that when deformations were transferred from the numerical model to the experimental setup, the hybrid test was only stable when the stiffness of the numerical model was higher than the test specimen. The hybrid test gave similar results as a numerical simulation of the full structure. The deviation between the two was primarily due to the
response of the specimen in the hybrid test being one load step behind the numerical model.

1 Introduction

In hybrid testing a structure is emulated by combining the response of an experimental- and numerical substructure. The main part of the emulated structure is modelled in a simulation and a part of special interest is tested in an experiment [1], [2]. When combining the response of the two, the behaviour of the full emulated structure can be obtained. With this technique, the response of a given substructure displaying non-linear behaviour e.g. buckling, fracture, can be investigated when exposed to the effect of the remaining structure, without conducting full-scale experiments.

Hybrid testing has previously been applied to investigate seismic protection of building structures [3], [4], [5]. For this application the load bearing structure has been simulated in a numerical model while damping fixtures has been tested experimentally, e.g. elastomer [6], stud types [7], [8], magneto-rheological [4], [9], [10]. These tests were dynamic and the focus was therefore to minimize the time lack between the numerical- and experimental component. This has been done by optimization of e.g. the numerical algorithms [11], [12], [13], and the actuator response [14], [15].

In all of these tests the numerical- and experimental component has been two separate – typically simply connected - structural components and this setup is referred to as multi-component hybrid testing. If hybrid testing is applied to a single-component structure e.g. wind turbine blade, boat hull etc. the boundary conditions between the numerical- and experimental substructure becomes more complicated. This is because the two substructures share boundaries along an edge of a structure instead of e.g. a clearly defined hinge as in the case of a hybrid test with a magneto-rheological damper [4], [9], [10]. This results in single-component hybrid testing having continuous boundaries between the two substructures, resulting in – in principle - an infinite amount of Degrees-Of-Freedom (DOF), compared to multi component hybrid testing where only a limited number of DOFs are present [1], [16]. It is therefore more complicated to monitor and control the deformations of the experimental substructure in a single-component hybrid test. This emphasizes the need for advanced measuring techniques to enable high-precision control of the experimental setup, as presented in [17].

The scope of this paper is to introduce and verify a sound base for single-component quasi-static hybrid testing. Digital Image Correlation (DIC) was implemented as a method to measure deformations to be used in the control loop. A quasi-static hybrid test on a multi component frame structure was conducted to reduce the complexity in verifying the software capabilities when handling the test response and theory. Here the numerical component was a Finite Element (FE) model of a simple frame structure and the experimental specimen a composite beam loaded in three point bending.

2   Hybrid Testing Communication Loop

The Quasi-static hybrid testing platform provides the capability to experimentally test a substructure of interest while simulating the remainder in a numerical model. The software is capable of: executing a FE-model, operating the hydraulic actuators through a multi-axial Proportional-Integral-Derivative (PID) controller and acquire data from several gauges on the test setup. The platform is operated by LabVIEW 8.6 and is executed in a state machine [18] presented in Figure 1.

An external force is applied to the numerical model (**1**) and the equivalent displacement at the shared boundary calculated for the numerical substructure in (**2**). This displacement is transferred to the experimental substructure by the hydraulic actuators in (**3**) controlled by a feedback signal acquired on the test specimen to omit the effect of compliance in the load train cf. [17]. Finally, the restoring force – i.e. the reaction force from the test specimen - in the shared boundary of the experimental substructure is fed back to the shared boundary of the numerical substructure in order to achieve equilibrium at the interface between the two. The loop is repeated by defining the next load increment in (**1**).

2.1   Numerical substructure (Part A)

The numerical substructure executed by (**2**) in Figure 1 is established through a link between LabVIEW 8.6 and ANSYS 12.1. The steps included in the communication between the two applications are presented in Figure 2.

The FE-model is defined through the ANSYS Parametric Design Language (APDL-script) which defines geometry, material properties, loads etc. The variable parameters in the APDL-script: external load P_{ext} and restoring force in the shared boundary R_n (see Figure 5) are identified and updated by (**1**). The APDL-script is executed in (**2**) by the ANSYS software through the windows command prompt. The output data is returned in a text file and the displacement at the shared boundary extracted by (**3**).

2.2 Experimental substructure (Part B)

The experimental substructure operated by (**3**) in Figure 1 is established through a link between LabVIEW 8.6 and two independent systems: the hydraulic actuator and external Data Acquisition (DAQ) system. The displacement controlled hydraulic actuator is operated through a MTS FlexTest 60 controller [19] by the TCP/IP port using a dynamic link library (DLL) [20]. The external DAQ system collects data from the measuring device DIC [21]. The steps in the communication between LabVIEW, PID-controller and external measuring device are represented in Figure 3.

The control loop is initiated in (**1**) by prescribing a displacement input to the PID-controller. Operated by the LVDT in the actuator the piston is moved towards the end level in a monotonic motion with a predefined deformation rate by (**2**). When the predefined displacement is reached the data from the load cell along with the signal from the DIC measuring device are acquired by (**3**). By comparing the deformation input with the actual response of the specimen a deviation is derived. If the deviation is within a given error tolerance the control loop is ready to receive the next deformation input in (**1**). If the deviation exceeds the error tolerance the actuator is moved in the direction necessary to reduce the error with a magnitude equal to the deviation. This is achieved by repeating the entire loop from (**2**) – (**4**) until a deviation below the error tolerance is achieved.

3 Hybrid Testing Setup

A somewhat simple multicomponent frame structure presented in Figure 4 is studied to reduce the complexity in verifying the software capabilities.

The emulated structure is separated in a numerical- and experimental component. Each component along with the coupling between them is illustrated in Figure 5.

The shared boundary between the two components is defined by a discrete point with two DOFs: translation in the y- and x-direction. With the assumption of having relatively small displacements the translation in the x-direction is neglected. The global stiffness of the numerical- and experimental component named S_A and S_B respectively is defined cf. eq. (1).

$$S_A = \frac{P_{ext}}{d_n} \quad \text{and} \quad S_B = \frac{R_e}{d_e} \tag{1}$$

The global stiffness of the numerical component is 4.94 times higher than the test specimen in the shared boundary.

3.1 Experimental component (Part B)

The experimental component consists of a Glass Fibre Reinforced Polymer (GFRP) beam loaded in three point bending. The specimen has the cross sectional width and height of 45mm and 19mm respectively and includes 22 unidirectional plies of fibre mats type: L1200/G50F-E06-A from Devold AMT with a nominal area weight of $1246g/m^2$. Five specimens are produced by vacuum infusion with an epoxy resin type: Airstone 760E mixed with an Airstone 776H hardener from Dow Chemicals Company. The fibre fraction is 55% [22] with the fibre mats oriented in the x-direction cf. Figure 7. The E-modulus in the direction of the fibres is by three point bending found in the range: 38.5-43.3GPa for the five specimens.

3.2 Numerical component (Part A)

The numerical component is discretized in a FE-model using an 8-node plane element with two DOFs in each node: translation in the x- and y direction. The bar connecting the numerical- and experimental component is defined by a 2-node beam element with three DOFs in each node: translation in the x- and y-direction and rotation around the z-axis. When the beam- and plane element is connected the rotation DOF is not

transferred to the plane element and the charnier is thereby obtained.

4   Three point bending

The experimental component is loaded in a 4-column MTS 810 axial test station with an axial servo-hydraulic actuator model: 244.22 which provide a maximum force of ±100kN with a stroke of ±33.00mm. The actuator is operated by a servo valve model 252.24C-04 with a capacity of 10l/s. The displacement of the actuator is measured by a linear variable differential transducer (LVDT) and the force measured by an MTS load cell model 661.19E-04 with a max capacity of 25kN. The test station is operated through a MTS FlexTest 60 PID-controller. The test rig has a loading- and support nose of 40mm - and 25mm diameter respectively cf. Figure 7. The motion of the measurement points (see Figure 7) are tracked by the commercial DIC system: ARAMIS by Optical Measuring Techniques (GOM). The side of the test specimen has been applied a random speckle pattern of white background with black dots. The resolution of the DIC sensors is 4 megapixels and the lenses are type: Titanar with a 20mm focal length. The images are divided into interrogation cells of 15x15 pixels with a shift of 2 pixel. The measuring field is 330x330mm^2 calibrated with a 250x200mm^2 calibration panel. The precision and accuracy for each measurement point obtained by the DIC system is determined to an RMS of 0.002mm and 0.009mm respectively. The accuracy of the DIC setup is evaluated by a micrometer of the type: Mitutoyo - series 164 in the range 0-50mm. The full setup of the test station including: specimen mounted in the three point bending rig and DIC camera is presented in Figure 7.

The position and numbering of the DIC measurement points along with the overall dimension of the specimen and three point bending setup is presented in Figure 7.

5   Test result

Five GFRP specimens are tested in a quasi-static multi-component hybrid testing setup presented in Figure 5. With the hydraulic actuator operated by a feedback signal acquired on the experimental substructure by DIC an error tolerance of 0.01mm is obtained cf. Figure 3. The system is loaded within the linear elastic regime by an external force P_{ext} in increments of 900N ranging from 0 to 18kN. The equivalent vertical displacement of the shared boundary is 0 to 6mm.

5.1   Hybrid Test

The hybrid test is verified by comparing the structural response in three simulations: hybrid test, full FE-model and analytical hybrid test. In the hybrid test, Part A in Figure 5 is modelled numerically and Part B is tested experimentally. In the full FE-model, Part A and B are both modelled numerically cf. figure 4. Here, the experimental component is assigned the same bending stiffness as found from a three point bending test, cf. chapter 3.1. In the analytical hybrid test Part A is modelled numerically and Part B is calculated analytically by Bernoulli-Euler theory. Here, the bending stiffness is the same as found in chapter 3.1. For test specimen four the deformation of the sheared boundary is presented as a function of the external force P_{ext} in figure 8a. To evaluate the deviation between the three simulations the discrepancy between the hybrid test, full FE-model and analytical hybrid test is presented in Figure 8b. The load step frequency of the hybrid testing loop in figure 1 is 0.09Hz.

From Figure 8, good correlation between the three simulations is achieved. A displacement error of 0.038mm between the full FE-model and analytical hybrid test is observed cf. figure 8b. This deviation is due to the restoring force in the hybrid test being one load step behind the numerical simulation of the full structure. The maximum discrepancy between the full FE-model and hybrid test is found to 0.034mm cf. figure 8b. Here the deviation is

caused by both the restoring force in the hybrid test being one load step behind the numerical simulation of the full structure along with other sources of error in the experimental component. The discrepancy between the full FE-model and hybrid test named displacement error (hybrid) and full FE-model and analytical hybrid test named displacement error (FEM) are presented in Table 1 for the remaining four specimens.

The relative error for each displacement error is given with respect to the total displacement of the shared boundary.

5.2 Test of Stability

The stability of the hybrid testing communication loop is affected by the ratio of the global stiffness in the shared boundary for the numerical- and experimental substructure, named S_A and S_B respectively, cf. eq. (1). For this reason a parametric study of the stiffness ratio between the experimental- and numerical substructure is performed. In this study the numerical component (part A, Figure 5) is defined in a FE-model while the response of the experimental component (part B, Figure 5) is calculated analytically from a Bernoulli-Euler assumption. The response at the shared boundary as a function of the external load P_{ext} is presented in Figure 9.

From Figure 9, the restoring force in the shared boundary become unstable when $S_A < S_B$. The instability is amplified when the ratio between S_A and S_B is increased. The phenomenon is avoided when the global stiffness of the numerical model is equal or higher than the experimental specimen ($S_A \geq S_B$). In the hybrid test performed in this paper the stiffness of the numerical substructure S_A is 4.94 times higher than the stiffness of the experimental substructure S_B. The hybrid loop is therefore stable. If the hybrid testing communication loop was inverted meaning that: the numerical- and experimental substructure receives a deformation- and force input respectively, instability is avoided if ($S_A \leq S_B$).

6 Discussion

Some discrepancies between the hybrid test and full FE-model was observed cf. Figure 8 and Table 1. This discrepancy is primarily due to the restoring force in the hybrid test being one load step behind the numerical simulation of the full structure cf. Table 1. This results in the overall structure displaying a lower stiffness than in the full finite element simulation. This source of error can be minimized by decreasing the size of the load step. It could also be minimized by predicting a restoring force. However, the efficiency of this method is dependent on the material behaviour of the specimen. In this study, the specimen was linear elastic making it easy to predict. However, if the test was performed on a specimen with non-linear behaviour e.g. plasticity, buckling etc. the response is harder to estimate. This is usually the case when doing hybrid testing, since the benefit of the method is that a part of a structure displaying unpredictable response can be analysed without testing the full structure [5].

The stability of the algorithm was investigated for different stiffness ratios between the numerical model and experimental structure. It was found that the hybrid test was stable when the stiffness of the numerical model was stiffer than the physical specimen, $S_A > S_B$. It was also shown that if the hybrid testing communication loop is inverted (see Figure 5) the opposite was the case. This is in general not an issue in hybrid testing, since tests are usually performed on large structures with high stiffness compared to the structural component of interest; cf. seismic testing of dampers in buildings [4], [9], [10]. However, one must consider this issue when applying hybrid testing to other types of systems, where the experimental substructure has stiffness higher than, or close to the numerical model. This issue could be addressed by predicting a restoring force for the next load step.

DIC was in this research implemented as a technique to acquire coordinates of three measurement points along the test specimen surface

cf. Figure 7. By implementing these measurements in a control loop (see Figure 3) the source of error being slack and deformations in the load train is neglected [23] [24]. Other essential data for handling of the coupling between the substructural parts could include e.g. strain measurements [25]. This could be done on the specimen surface by full field measurements, strain gauges, etc. The GFRP specimen also allows internal strain measurements by Fibre Bragg Gratings (FBG) to include stress concentrations and residual stresses in the specimen [22].

7   Conclusion

A hybrid test was performed and the response compared to a finite element simulation of the full structure. The comparison showed a small deviation primarily caused by the restoring force in the hybrid test being one load step behind the numerical simulation of the full structure. The hybrid testing setup in this study was used to prove the functionality of the hybrid testing communication loop and implement the DIC measurements to control the actuator. In the future the hybrid testing platform will be developed to handle single component structures with more advanced geometry e.g. wind turbine blades.

8   Acknowledgement

References

[1]   X. Shao, A. M. Reinhorn and M. V. Sivaselvan, "Real-Time Hybrid Simulation Using Shake Tables and Dynamic Actuators," *Journal of Structural Engineering,* vol. 137,

no. 7, pp. 748-760, 2011.

[2]   O. S. Bursi, A. Gonzalez-Buelga, L. Vulcan, S. A. Neild and D. J. Wagg, "Novel coupling Rosenbrock-based algorithm for real-time dynamic substructure testing," *Eartquake Engineering and Structural Dynamics,* vol. 37, pp. 339-360, 2008.

[3]   K. Takanashi and M. Nakashima, "Japanese Activities on On-line Testing," *Journal of Engineering Mechanics,* vol. 113, no. 7, pp. 1014-1032, 1987.

[4]   C. Chen, J. M. Ricles, T. L. Karavasilis, Y. Chae and R. Sause, "Evaluation of a real-time hybrid simulation system for performance evaluation of structures with rate dependent devices subjected to seismic loading," *Engineering Structures,* vol. 35, pp. 71-82, 2012.

[5]   A. Bonelli and O. S. Bursi, "Generalized-alpha methods for seismic structural testing," *Earthquake Engineering ad Structural Dynamics,* vol. 33, pp. 1067-1102, 2004.

[6]   T. L. Karavalis, J. M. Ricles, R. Sause and C. Chen, "Experimental evaluation of the seismic performance of steel MRFs with compressed elastomer dampers using large-scale real-time hybrid simulation," *Engineering Structures,* vol. 33, pp. 1859-1869, 2011.

[7]   M. Ito, Y. Murata, K. Hoki and M. Nakashima, "Online Hybrid Test on Buildings with Stud-Type Damper Made of Slitted Steel Plates Stiffened by Wood Panels," *Procedia Engineering,* vol. 14, pp. 567-571, 2011.

[8]   A. Jacobsen, T. Hitaka and M. Nakashima, "Online test of building frame with slit-wall dampers capable of condition asessment," *Journal of Constructional Steel Research,* vol.

66, pp. 1320-1329, 2010.

[9] Y. Z. Lin and R. E. Christenson, "Comparison of Real-time Hybrid Testing with Shake Table Test for an MR Damper Controlled Structure," *American Control Conference,* pp. 5228-5233, 2009.

[10] J. E. Carrion, B. F. Spencer Jr. and B. M. Phillips, "Real-Time Hybrid Testing of a Semi-Actively Controlled Structure with an MR Damper," in *American Control Conference,* Hyatt Regency Riverfront, St. Louis, MO, USA, 2009.

[11] R.-Y. Jung, P. B. Shing, E. Stauffer and B. Thoen, "Performance of a real-tme pseudodynamic test system considering nonlinear structural response," *Earthquake Engineering and Structural Dynamics,* vol. 36, pp. 1785-1809, 2007.

[12] G. Mosqueda and M. Ahmadizadeh, "Combined implicit or explicit integration steps for hybrid simulation," *Earthquake Engineering and Structural Dynamics,* vol. 36, pp. 2325-2343, 2007.

[13] B. Wu, G. Xu, Q. Wang and M. S. Williams, "Operator-splitting method for real-time substructure testing," *Earthquake Engineering and Structural Dynamics,* vol. 35, pp. 293-314, 2006.

[14] M. Verma and J. Rajasankar, "Improved model for real-time substructuring testing system," *Engineering Structures,* vol. 41, pp. 258-269, 2012.

[15] M. Nakashima and N. Masaoka, "Real-Time On-Line Test for MDOF Systems," *Earthquake Engineering and Structural Dynamics,* vol. 28, pp. 393-420, 1999.

[16] C. Chen, J. M. Ricles, T. M. Marullo and O. Mercan, "Real-time hybrid testing using unconditionally stable explicit CR integration algorithm," *Earthquake Engineering and Structural Dynamics,* vol. 38, pp. 23-44, 2009.

[17] J. Waldbjørn, J. Høgh, J. Wittrup-Schmidt, M. Nielsen, K. Branner, H. Stang and C. Berggreen, "Strain and Deformation Control by Fibre Bragg Grating and Digital Image Correlation," *Strain,* (to be submitted).

[18] R. Bitter, T. Mohiuddin and M. Nawrocki, LabView Advanced Programming Techniques, Boca Rotan, Florida, USA: CRC Press, 2001.

[19] MTS, "MTS Systems Corporation, FlexTest Controllers," MTS Systems Corporation, 8 Oktober 2011. [Online]. Available: https://www.mts.com. [Accessed 8 Oktober 2011].

[20] MTS, LabVIEW Programming Libraries: Model 793.00 Software, MTS Systems Corporation, 2009.

[21] GOM, ARAMIS - User Manual - Software, Braunschweig, Germany: GOM, 2006.

[22] M. W. Nielsen, J. Wittrup-Schmidt, J. Hattel, J. H. Høgh, J. P. Waldbjørn, J. Andersen and T. L. Markussen, "In-situ measurements using FBGs of process-induced strains during curing of thick glass/epoxy laminate plate: Experimental results and Numerical modeling," *Composites.*

[23] X. Fayolle, S. Galloch and F. Hild, "Controlling Testing Machines with Digital Image Correlation," *Experimental Techniques,* vol. 31, no. 3, pp. 57-63, 2007.

[24] J. Waldbjørn, J. Høgh, J. Wittrup-Schmidt, M. Nielsen, K. Branner, H. Stang and C.

Berggreen, "Strain and Deformation Control by Fibre Bragg Grating and Digital Image Correlation," *Strain,* To be submitted.

[25] U. C. Mueller, T. Zeh, A. W. Koch and H. Baier, "Fiber Optic Bragg Grating Sensors for High-Precision Structural Deformation Control in Optical Systems," *SPIE,* vol. 6167, 2006.
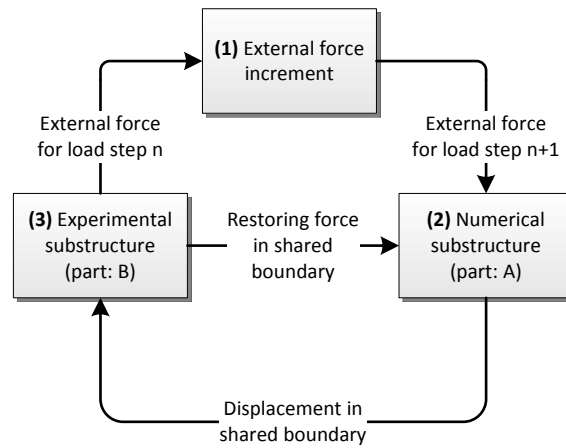
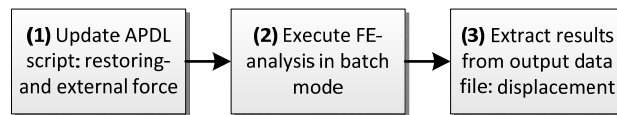**Figure 1: Dataflow in the quasi-static hybrid testing communication loop**

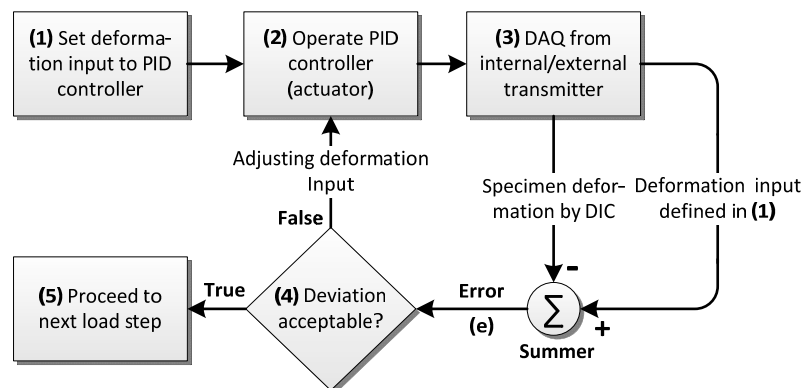**Figure 2: Dataflow in the LabVIEW and FE-analysis communication (Part A)**

Figure 3: Dataflow in the closed single input-single output control loop (Part B)

Figure 4: Emulated structure
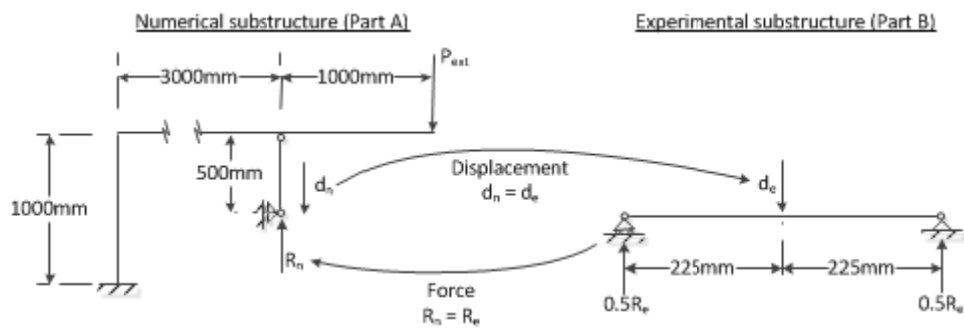
Figure 5: The emulated structure separated in: a) numerical component and b) experimental component
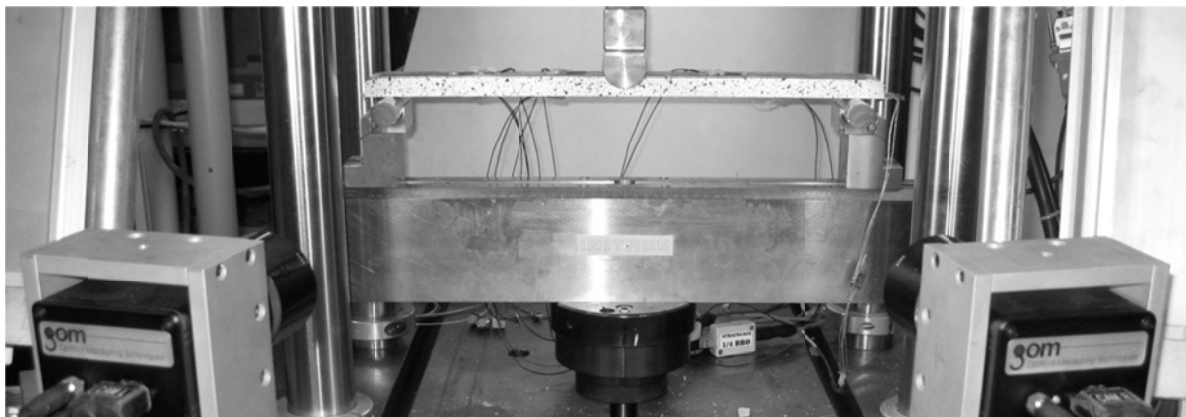

Figure 6: The three point bending setup with GFRP beam and speckle pattern
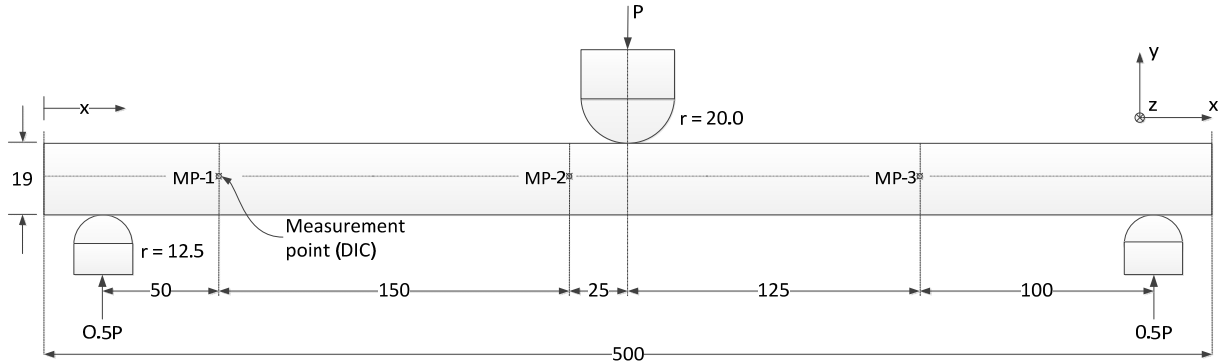
Figure 7: Dimensions of test setup and specimen along with numbering and location of DIC measurement points
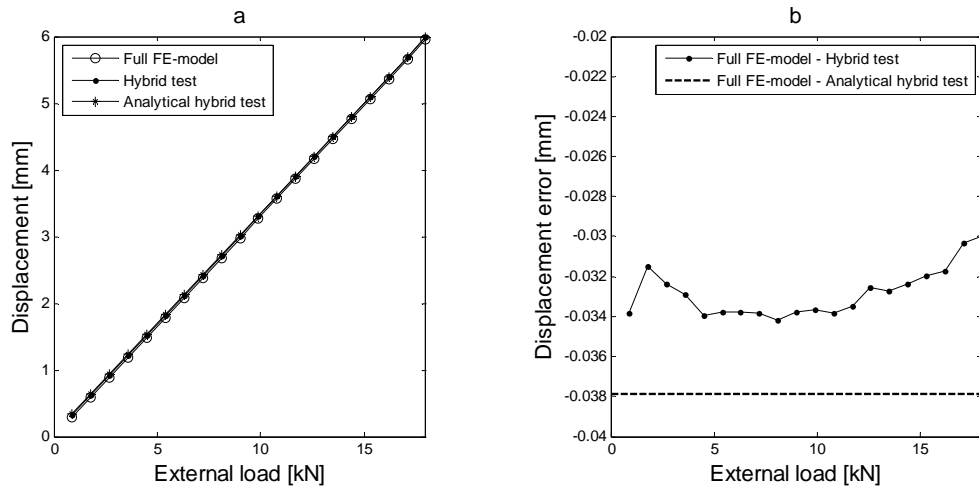

Figure 8: a) load – deformation relation at the loading point and b) discrepancy between the response of the full FE-model and hybrid test

Table 1: Displacement- and relatively error for test specimen 1 to 5

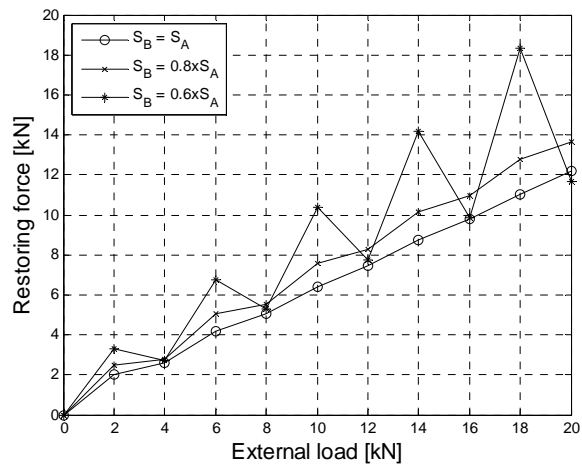| Beam number [-]	Displacement Error (FEM) [mm]	Relatively error [%]	Displacement Error (Hybrid) [mm]	Relatively error [%]
1	0.048	0.83	0.042	0.72
2	0.044	0.75	0.038	0.65
3	0.043	0.74	0.038	0.64
4	0.038	0.64	0.034	0.57
5	0.047	0.81	0.041	0.69

Figure 9: Restoring force in the shared boundary as a function of the external load